Nozzle Geometry Effects in Liquid Jet Array Impingement

Brian P. Whelan, Anthony J. Robinson

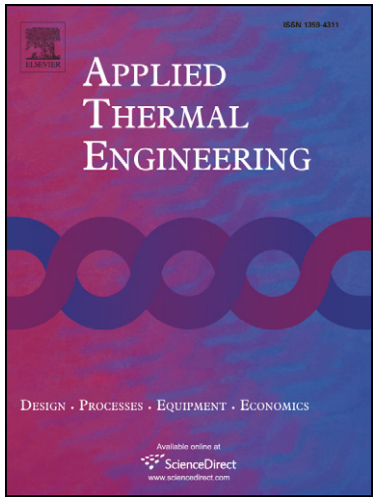

Nozzle Geometry Effects in Liquid Jet Array Impingement

Brian P. Whelan, Anthony J. Robinson

PII: S1359-4311(08)00443-2
DOI: 10.1016/j.applthermaleng.2008.11.003
Reference: ATE 2655

To appear in: *Applied Thermal Engineering*

Received Date: 21 April 2008
Revised Date: 29 October 2008
Accepted Date: 4 November 2008

Please cite this article as: B.P. Whelan, A.J. Robinson, Nozzle Geometry Effects in Liquid Jet Array Impingement, *Applied Thermal Engineering* (2008), doi: 10.1016/j.applthermaleng.2008.11.003

Nozzle Geometry Effects in Liquid Jet Array Impingement

Brian P. Whelan, Anthony J. Robinson[1]

Department of Mechanical and Manufacturing Engineering,
Trinity College Dublin, Ireland
CTVR (Centre for Telecommunications Value-Chain Research)
[1]Corresponding author: Tel.: +353-1-896 3919; fax: +353-1-679 5554
Email: arobins@tcd.ie

Abstract

The use of impinging liquid jets in electronics thermal management is attracting some consideration due to their very high heat transfer coefficients, hot spot targeting capabilities and moderate hydraulic power requirements. In this investigation an experimental study of the cooling capabilities of impinging water jet arrays is presented. Of particular interest here is the influence that the inlet and outlet geometries have on the thermal-hydraulics of jet impingement heat transfer with the aim of determining practical configurations in which heat transfer to the impinging jets is increased and/or the hydraulic pumping power is decreased. For a square array of 45 jets of fixed 1.0 mm diameter and fixed interjet spacing of 5 mm, six different nozzle geometries were investigated. The arrays impinged normally upon a heated circular copper surface of 31.5 mm diameter for a nominal heat flux of 25.66 W/cm^2. Each array was tested under confined-submerged flow conditions with a constant jet-to-target spacing of 2.0 mm as well as free-surface conditions with a constant jet-to-target spacing of 20 mm. All nozzles were tested for a Reynolds number range of approximately $800 \leq Re_{dn} \leq 10000$. It has been found that the confined-submerged tests yield greater heat transfer coefficients compared with their free jet counterparts. Chamfering and contouring the nozzle inlets showed significant decrease in the pressure drop across the nozzle plate whilst chamfering and contouring the exit showed moderate gains in the surface averaged heat transfer coefficient. Nozzles that provide the highest heat transfer for a given hydraulic pumping power are identified for each free-surface and confined-submerged scenarios.

Key words: Electronics cooling; Liquid Jet impingement; Nozzle Geometry; Pumping Power.

1. Introduction

Unwanted heat is generated by electronic devices which can adversely affect their performance and reliability. The current trend of miniaturizing electronic components coupled with increases in transistor density and processing speeds has lead to continual increases in the surface heat flux levels. If the thermal management is inadequate unacceptable temperature levels may be reached which can adversely affect its performance, reliability and lifespan. At present heat fluxes as high as 50 W/cm^2 have been reported in high-end commercial applications and in the coming years this value is expected to exceed 100 W/cm^2 [1].

Air cooled fan-fin techniques are widely used in the cooling of electronic components. Conventional fan-fin cooling technologies are well characterized, reliable and inexpensive. However, this technology has nearly reached it maximum cooling and acoustic thresholds while at the same time demanding a disproportionate space claim at board level compared with the size of the electronic component it is cooling. This has caused severe thermal management and packaging issues and is becoming one of the major bottlenecks in the advancement of electronics technology [1]. Consequently, there is high demand by electronic packagers for alternative and high performance thermal management technologies.

The use of impinging liquid jets as a viable method of heat removal is one area receiving some consideration. Impinging liquid jets have already found extensive use in industrial applications for purposes such as the thermal treatment of metals and the cooling and turbine blades [2, 3]. Their popularity derives from the fact that impinging liquid jets possess one of the highest known single phase heat transfer coefficients. When used in arrays they are ideal for global cooling of electronic components since the liquid jet arrays facilitate the desirable characteristic very high heat flux removal at small heater surface-to-coolant temperature differences. Further to this the pressure

drop across the nozzle required to form the jet is not necessarily coupled with the heat transfer mechanism at the impingement surface. This establishes the attractive possibility of an optimal nozzle configuration in which, for a required heat transfer coefficient, volumetric flow rate and pumping power can be minimized [4].

Impinging jets can be classified as either free-surface or submerged. Submerged jets exude into an space containing the same liquid at rest and can configured as confined or unconfined depending on the jet-to-target spacing. In a submerged configuration, the interaction of the issuing jet and the stagnant fluid leads to entrainment in the shear zone and the development of a potential core near the jet centreline. The potential core is the region in which the velocity of the jet remains largely unaffected by the spreading of the jet due to entrainment and has been found to be typically between five and eight nozzle diameters in length [5]. In the confined case, the fluid heated by the target plate can in some instances get recirculated and get entrained back into the impinging jet [6]. This causes the formation of a toroidal recirculation zone in the outflow region [6]. In an unconfined configuration, such the case when jets are issuing from long tubes, the jet interacts with the ambient and otherwise quiescent surroundings and have associated with them higher heat transfer coefficients as the heated liquid is not entrained back into the jet as is sometimes the case for confined jets [6, 7]. The point at which jets differentiate between fully confined and fully unconfined will likely depend on many factors including but not limited to Re, H/d_n, surface drainage and surface topology, although this has not been fully characterized though some progress has been made [7]. In a free-surface jet configuration, the liquid is discharged from the nozzle into an ambient gas, typically air, before impinging upon the target surface. Therefore, entrainment of surrounding fluid can be considered negligible so that a potential core is not relevant in this case. Due to the previously mentioned trend of component miniaturization, the available

space for the cooling device will likely be very restricted. As such, the confined-submerged configurations will likely be the one implemented in an impinging jet cooling package.

Many studies have investigated single circular impinging jets for both submerged and free-surface jet configurations and have provided information regarding the heat transfer for fluids such as air, FC-77 and water [5, 8-17]. The local heat transfer coefficient distribution has generally been found to be bell-shaped in nature. The maximum heat transfer coefficient occurs at or near the stagnation point and decreases with radial distance from this point. Secondary peaks in local Nusselt number have been reported by several investigators, most recently being O'Donovan and Murray [16] who reported that for their specific test configuration prominent secondary peaks in the local Nusselt number occurred at approximately r/d_n = 1.6 for small nozzle-to-surface separations (H/d_n ~0.5). The peaks were attributed to transition to turbulence in the wall jet region. It was also reported that, as H/d_n increased, the magnitude of the secondary peak decreased and its location moved further away from the stagnation point. The locations of these secondary peaks in the heat transfer coefficient were found to be dependant on the impinging jet and more specifically the degree of spreading of the jet. As H/d_n increased it was reasoned that a greater amount of radial spreading occurs leading to an increase in the size of the region in which the wall jet feels the suppressing effects of the impinging jet. This caused the secondary peak to occur at greater radial distances from the geometric centre as transition to turbulence in the wall jet region is delayed. Using Laser Doppler Anemometry, the location of these peaks was shown to coincide with peaks in axial velocity fluctuations.

The magnitude and distribution of the heat transfer coefficient has been found to be dependant on a number of parameters including, but not limited to, the Prandtl number (Pr), Reynolds number (Re), jet-to-target spacing (H/d_n), jet diameter (d_n),

nozzle thickness to diameter ratio (t/d_n) and the physical geometry of the jets and heater surface [18, 19]. Compared to single jet impingement, the heat transfer and flow characteristics of jet arrays have received much less attention in the open literature although some work exists [18, 20]. The primary advantage of arrays of multiple jets is the creation of multiple stagnation zones with exceptionally high local heat transfer coefficients. Depending on aspects such as interjet spacing and cross flow conditions, high local surface heat transfer coefficients can be maintained over the entire surface. This can result in very high surface average heat transfer coefficients and more uniform surface temperature distributions which is a particularly desirable property of an electronics cooling package.

Womac et al [21] investigated both confined-submerged and free-surface jet impingement heat transfer, using water and FC-77 as the coolants. Arrays of 2x2 and 3x3 circular jets were tested for jet diameters of 0.513 mm and 1.02 mm over various jet-to-jet spacing. The heat transfer to the free-surface jets was found to be independent of the jet-to-target spacing in the range $5 \leq H/d_n \leq 10$. When the volumetric flow rate was held constant, it was observed that the heat transfer increased with decreasing values of d_n and N, which was attributed to increases in the jet velocity. When the flow rate, d_n and N were held constant, the heat transfer was found to increase with decreasing values of jet-to-jet spacing, with interaction between neighbouring cells and/or a possible reduction in the wall jet region associated with each jet possible explanations of this enhancement. Experiments conducted for the confined-submerged liquid jet arrays found that the heat transfer coefficient was somewhat insensitive to jet-to-target spacing within the range of $2 \leq H/d_n \leq 4$ due to the target surface being within the potential core of the issuing jets. Under similar conditions, the heat transfer to the submerged jets was found to exceed, or approximately equal, that to their free jet counterparts.

The effect of jet-to-jet spacing for jet arrays was more closely examined by Pan and Webb [22]. The local heat transfer distribution was investigated with water as the test fluid for a 9 jet-in-line array and a 7 jet staggered array over various jet-to-jet spacing between $2 \leq S/d_n \leq 8$. For the central jet module, the stagnation point heat transfer coefficient was found to be independent of jet-to-jet spacing. Conversely, a dependence on the jet-to-target spacing was discovered. By increasing the dimensionless jet-to-target spacing (H/d_n) from 2 to 5, the flow condition was observed to change from a confined-submerged jet flow to a free-surface jet flow. Secondary stagnation heat transfer regions of significant magnitude were also observed midway between adjacent jets. The interaction between neighbouring jets was put forth as an explanation for this occurrence.

The more recent work of Fabbri and Dhir [4] appears to be one of the first to consider both heat transfer to the jet arrays and the associated pressure drop across the jet nozzle plate. The study investigated free-surface microjet arrays of water and FC40 within a Reynolds number range of $73 \leq Re_{dn} \leq 3813$, and jet diameter range of $65\mu m \leq d_n \leq 250\mu m$. Increases in Re_{dn} and Pr, as well as decreases in S/d_n, were observed to lead to improvements in the average surface heat transfer coefficient. The minimum pumping power requirement for a given required heat dissipation was found to be dependant upon the interjet spacing and jet diameter. A trend was observed in which the optimal jet diameter was found to increase with increasing interjet spacing, with a jet spacing of 5 mm and jet diameter of 775 μm proving to be ideal. It was also noted that heat transfer to the microjet arrays was considerably larger than for miniature and mesoscale jets for identical volumetric flow rates.

Robinson and Schnitzler [23] conducted experiments investigating the impingement of water jet arrays under both free-surface and submerged conditions. In this work a large population of jets was used which induces cross flow which is known

to influence the heat transfer [24]. Jet diameters of 1 mm were used, with a jet-to-jet spacing range of $3 \leq S/d_n \leq 7$. Heater surface-averaged heat transfer and pressure drop data was recorded for a dimensionless jet-to-target spacing range of $2 \leq H/d_n \leq 30$ and Reynolds number range of $650 \leq Re_{dn} \leq 6500$. For the submerged jets, it was found that heat transfer was insensitive to jet-to-target spacing changes in the range of $2 \leq H/d_n \leq 3$. A monotonic decrease in heat transfer was observed with increasing jet-to-target spacing in the range of $5 \leq H/d_n \leq 20$. It was reported that, for a constant Reynolds number, increasing the jet-to-jet spacing incurred a detrimental effect on heat transfer. It was also found that a stronger dependence on jet-to-jet spacing was encountered for smaller jet-to-target spacing. Free-surface jets were observed to behave as submerged jets within the range of $2 \leq H/d_n \leq 10$. Beyond this value, entirely free jet flow occurs with the heat transfer coefficient showing marginal improvement with increasing jet-to-target spacing. Robinson and Schnitzler correlated their heat transfer data for free-surface jets as:

$$\frac{Nu_L}{\mathrm{Pr}^{0.4}} = 7.8\,\mathrm{Re}_{d_n}^{0.49} \exp\left(-0.025\frac{S}{d_n}\right) \tag{1}$$

A Nusselt number correlation for the confined-submerged data, valid between $2 \leq H/d_n \leq 3$, was also presented as:

$$\frac{Nu_L}{\mathrm{Pr}^{0.4}} = 23.39\,\mathrm{Re}_{d_n}^{0.46}\left(\frac{S}{d_n}\right)^{-0.442}\left(\frac{H}{d_n}\right)^{-0.00716} \tag{2}$$

At jet-to-target spacing below $H/d_n=3$ the confined-submerged jets provided higher heat transfer coefficients for lower pumping power cost compared with free jets. It was also noted that under confined-submerged conditions, decreasing the interjet spacing, and therefore increasing the number of jets, decreased the pumping power requirement for a given heat transfer coefficient.

Royne and Dey [25] investigated the effect of nozzle geometry on the heat transfer and pressure drop to confined-submerged jet arrays over a Reynolds number range of $1000 \leq Re_{dn} \leq 7700$. Four different geometries were investigated with sharp-edged nozzles experiencing the largest heat transfer coefficient and countersunk nozzles encountering the lowest. In terms of pressure drop, the same was again true with sharp-edged nozzles experiencing the greatest pressure drop and countersunk nozzles the lowest. These results were attributed to their respective favourable and unfavourable discharge coefficients. Two conventional straight nozzles were also examined and the array of greater plate thickness, and therefore longer development length, experienced a smaller pressure drop than its thinner counterpart. This was accredited to the formation of a separation bubble at the inlet, which reattached for the nozzle of greater thickness thus increasing the discharge coefficient. With regards to heat transfer for a given pumping power, it was reported that the sharp-edged and contoured nozzles both experienced enhanced performances in comparison to the conventional straight nozzle arrays. The sharp-edged nozzle array decreased the flow rate required for a given heat transfer, whilst the countersunk nozzle required an increased flow rate at a reduced pressure drop.

At present there is limited data available for the heat transfer and pressure drop associated with the impingement of liquid jet arrays. Further to this, few investigations on the influence of nozzle geometries deviating from the common straight, circular structure exist. This work is the natural progression of the works of Robinson and Schnitzler [23] and Royne and Dey [25] in which different inlet and/or outlet modifications are investigated with respect to the thermal-hydraulic performance of impinging liquid jet arrays. In particular, the use of state of the art 3D rapid prototyping allows for more complex geometrical configurations to be manufactured compared with previous works. Further to this, the influences of nozzle entrance and/or exit conditions

are investigated for both confined-submerged and free-surface jet configurations. The primary motivation for this work is that the thermal-hydraulics of impinging jet arrays plays an important role in their suitability for use in the electronics thermal management. Consequently, it is desired to ascertain whether enhancement over the conventional straight nozzle, with regards to the pumping power requirement for a given heat transfer coefficient, can be obtained.

2. Experimental Set-up

The surface averaged heat transfer coefficient and pressure drop characteristics of impinging free-surface and confined-submerged water jet arrays have been experimentally investigated. A total of six jet nozzle geometries, with varying inlet and outlet modifications, were tested for a Reynolds range of approximately $800 \leq Re_{dn} \leq 10000$. The jet diameter ($d_n$) was fixed at 1 mm and each array tested possessed a dimensionless interjet spacing (S/d_n) of 5. This resulted in each array containing 45 individual jets which impinged normally upon the target surface. The geometric characteristics of the nozzles tested are provided in Table 1. For the chamfered nozzles, the chamfered angle was 45° to the normal, with a depth of t/2 = 1.5 mm. The contoured nozzles were constructed using the conic round function with a 1.75 mm base radius and a conic parameter of 0.5 m [28]. The free-surface jets were investigated at a dimensionless jet-to-target spacing of $H/d_n = 20$. As shown in previous experimentation [23], the influence of H/d_n is small for free-surface jet impingement beyond approximately $H/d_n = 10$, hence the present results can be considered representative of a larger range of H/d_n values. In their experiments, Robinson and Schnitzler [23] observed that, for submerged jets, the largest average heat transfer coefficients occurred in the region of $2 \leq H/d_n \leq 3$. Consequently, a value of $H/d_n = 2$ was selected for the confined-submerged experiments in order to achieve the greatest

possible heat transfer. As depicted in Fig.1, the experimental apparatus consisted of a water delivery and monitoring system, as well as a test chamber which contained the jet array nozzle and heated impingement surface.

2.1 Flow delivery and monitoring system

The water flow loop illustrated in Fig. 1 used a pump to draw distilled and deionized water from a 20 L water reservoir. A constant water temperature was ensured through the installation of a coiled heat exchanger which was submerged within the reservoir. In order to eliminate the presence of particulates which may clog the jets, a 10 μm filter was fitted within the flow loop. The installation of two bypass valves facilitated the control of the water flow rate before it entered the rotameter bank. Satisfactory accuracy in the readings of the volumetric flow rate over a large enough flow range was ensured by equipping the flow loop with three rotameters of differing range (4-22 LPM ± 1.5%FS, 2-10 LPM ± 1.5%FS, 0-2 LPM ± 1.5%FS). A 1.5 mm diameter sheathed T-type thermocouple, coupled with a Fluke54II digital thermometer (±0.3°C), was used to measure and record the water temperature at the inlet of the test chamber. As depicted in Fig. 2, the water entered the test chamber through a 170 mm length of 19 mm inner diameter straight tubing that was expanded to a 70 mm long x 80 mm inner diameter plenum before being ejected through the jet nozzle plate. The jet nozzle plates were 3 mm thick and designed using a commercial 3-D CAD package. They were subsequently printed using an InVision™ 3-D Printer of 10 μm resolution. The interchangeable nozzle plates were attached to the plenum by eight screws with a crushed O-ring seal. The embedded photograph in Fig. 2 illustrates this arrangement.

2.2 Test chamber

The test chamber permitted the measurement of both the pressure differential across the jet nozzle plate and the surface average heat transfer coefficient from the heated block to the impinging water jets. The pressure drop across the nozzle plate was measured using a Digitron 2083P (0-2 bar ± {0.1% rdg + 0.1%FS}) differential pressure meter which was installed between two pressure taps located on either side of the jet nozzle.

As illustrated in Fig. 2, the metered heater block used in this study was made from a cylindrical bar of ultra pure oxygen-free copper. The upper surface of the block was machined flat and served as the heater surface with an exposed diameter of 31.5 mm. The diameter of the block was decreased slightly below the heater surface in order to provide sufficient space for the thermocouple wires to exit. This space also supplied an insulating air gap between the copper block and the stainless steel sleeve which was laser welded to the heater block to ensure a water-tight seal. An ample quantity of fibreglass insulation was wrapped around the outer periphery of the heater section in order to minimize radial heat loss and ensure one dimensional heat flow to the heater surface. A through hole, in which the cylindrical heater block was inserted, was machined into a 20 mm thick acrylic sheet. To aid drainage through the four 15 mm drainage ports, the heater surface protruded 5 mm above the acrylic sheet. In order to contain the water and ensure it flowed into the drainage ports, a 193 mm diameter by 300 mm long acrylic tube was fixed to the top side of the acrylic base plate. On passing through the drainage ports, the water was then gravity fed back to the reservoir.

Three 6.35 mm diameter by 44.45 mm long cartridge heaters were inserted into holes drilled into the bottom of the heater block to provide power to the device. A variable transformer was used to regulate the heat supplied which was set at 200 W for all tests. Two Metrix MX22 multimeters (0-400VAC ± 1% rdg, 0-10 A ± 2.5% rdg) monitored the current and voltage supplied to the heaters. The determination of the heat

flux and the surface temperature of the copper block was facilitated through the implementation of three E-type thermocouples of 1.0 mm diameter along the centreline of the cylindrical block. The top thermocouple was inserted 1.6 mm below the impingement surface with each subsequent thermocouple a further 9.5 mm beneath. A Fluke54II digital thermometer (±0.3°C) monitored all thermocouple readings, which were recorded once steady-state conditions were reached.

3. Data Reduction

The heat flux at the heater surface was assumed to be uniform and was calculated from using the expression,

$$q'' = k_{Cu} \left. \frac{dT}{dz} \right|_{\substack{best \\ fit}} \tag{3}$$

where k_{cu} is the thermal conductivity of the ultra pure copper evaluated at the average block temperature, and $dT/dz|_{best\ fit}$ is the linear regression fit of the centreline temperature measurement. As detailed in [26], the uncertainty in the heat flux measurement was determined to be ±4.1%. The surface temperature (T_s) was determined by linear extrapolation of the centreline temperature distribution to the surface,

$$T_s = T_t + (z_s - z_t)\left(\left. \frac{dT}{dz} \right|_{\substack{best \\ fit}} \right) \tag{4}$$

where z_s-z_t is the distance from the surface to the location of the top thermocouple. The average heat transfer coefficient at the heated surface was determined with the expression,

$$\bar{h} = \frac{q''}{(T_s - T_{jet})} \tag{5}$$

The post-calibrated temperature difference (T_s-T_{jet}) uncertainty was estimated to be 2%. Using the heat transfer coefficient calculated using Eq. 5 the surface-average Nusselt number was determined as,

$$Nu_L = \frac{\bar{h} L_c}{k_f} \tag{6}$$

where the characteristic length for the heater surface was chosen as L_c = D/2 = 15.75 mm and the thermal conductivity of the liquid was evaluated at the film temperature.

The jet Reynolds number was calculated using the average jet velocity as can be determined by knowledge of the total water flow rate, the total number of jets and the cross-sectional area of the jet. The jet velocity and thus the jet Reynolds number can then be calculated using the equations,

$$V_n = \frac{4\dot{V}}{N\pi d_n^2} \tag{7}$$

and,

$$\mathrm{Re}_{d_n} = \frac{V_n d_n}{v_{film}} \tag{8}$$

Based on the pressure drop data recorded, the friction factor was calculated using the expression,

$$f = \frac{\Delta P}{\left(\frac{1}{2}\rho V_n^2\right)\left(\frac{t}{d_n}\right)} \tag{9}$$

Table 2 lists the estimates of the experimental uncertainties for the main parameters.

4. Results and Discussion

Experimental data were obtained for each of the six arrays under both confined-submerged and free-surface conditions. The results for the straight nozzles are presented first to establish the baseline cases for comparison with the modified nozzle geometries. In order to keep the parametric range manageable whilst still providing

enough range for comparisons, a fixed interjet spacing of $S/d_n=5$ has been selected for all of the nozzle configurations studied. Further, for the confined submerged cases a fixed jet-to-target spacing of $H/d_n=2$ is chosen since Robinson and Schnitzler [23] showed that for $H/d_n>3$ the heat transfer tends to degrade sharply with increased jet-to-target spacing. Similarly, for the free-surface jet configuration a fixed jet-to-target spacing of $H/d_n=20$ has been used. Between approximately $15 \leq H/d_n \leq 30$ the jets can be considered fully unconfined and the heat transfer coefficient changes very little [23].

4.1 Straight Nozzle Results

The relationships between Reynolds number and Nusselt number for the straight nozzle arrays for both free-surface and confined-submerged conditions are presented in Fig. 3. Also included in the figure are the Robinson and Schnitzler [23] correlating equations. As evident from Fig. 3, the results obtained compare well with the Robinson-Schnitzler correlations and provides confidence in the experimental technique and validity of the measurements and data reduction technique used.

The confined-submerged results are seen to agree with the Robinson-Schnitzler correlation over the entire Reynolds number range investigated. The original correlation was developed for a Reynolds number range of $650 \leq Re_{dn} \leq 6500$, however the results obtained here suggest that the correlation may in fact be valid up to $Re_{dn} \approx 10000$. Compared with the free-surface jets the confined-submerged jets achieve larger surface averaged Nusselt number values over the entire Reynolds number range investigated although the two situations show a similar power law dependence on the Reynolds number. Local surface temperature measurements were not taken in this study. Even still it is speculated that the improved heat transfer is likely a result of the mechanisms described by Garimella and Schroeder [19] where for confined air jet arrays a notable enhancement in the local and area averaged heat transfer coefficient occurs for small

jet-to-target spacings. The reasoning posed was a combination of an increase in the turbulent intensity of the jet by mixing with the spent flow from neighbouring jets as well as a reduction in the entrainment of warm spent fluid back into the jet for small H/d_n which tends to increase jet performance.

In the case of the free-surface data, the Robinson-Schnitzler correlation shows agreement for low and moderate Reynolds numbers whilst the correlation tends to notably over-predict the data for $Re_{dn} > 6500$, which is outside the the Reynolds number range for which the correlation was developed. For arrays of free-surface water jets, Garrett and Webb [27] attributed this type of degradation in the heat transfer to the existence of a liquid layer on the heater surface. If surface drainage is not adequate the jets exiting the nozzle had to penetrate this liquid layer en route to striking the heater surface which diminished their effectiveness. Visual observation and digital photography confirmed that an apparent growth of the liquid layer on the surface began for volumetric flow rates above approximately 10 L/min (Re_{dn}~5000) due to inadequate drainage from the test chamber. Within the context of electronics thermal management this highlights a potential pitfall with regards to surface cooling with free-surface jet arrays if inadequate drainage is provided.

The relationships between Reynolds number and friction factors for the two configurations are illustrated in Fig. 4. Similar trends are measured for both the submerged and free jet arrays; however greater friction factors, and therefore pressure drops, are generally produced by the confined-submerged jets. This can be attributed to the jets exuding into a pool of water which provided greater resistance than the ambient air into which the free-surface jets exude.

4.2 Modified Nozzle Geometries: Free-Surface Results

Fig. 5 plots the relationship between surface averaged heat transfer coefficient and the volumetric flow rate for each of the modified nozzles under free-surface conditions. Embedded in the figure are the corresponding ratios of the heat transfer coefficients to that of the straight nozzle. The figure indicates that the chamfered and contoured inlet nozzles experience a notable increase in the heat transfer for small (<4 L/min) volumetric flow rates followed by a decreases in heat transfer coefficient of about 8% in the region of 5-10 L/min. For the higher flow rates their performance generally improves. Although the results presented here are for one test case, it must be noted that the trends observed were very repeatable and several tests were carried out to ensure this. For the low flow range it was observed that for the straight nozzles the distinct small diameter jets did not tend to form. Instead the water issuing from the nozzles broadened outward along the flat surface of the nozzle plate until they merged with a neighbouring jet(s) forming large laminar liquid jets with significant jet break-up. The lateral merging of jets is a surface tension effect which depends on the influence of liquid inertia forces to surface tension forces as characterized by the Weber number, ($We=\rho V_n^2/\sigma$). The situation observed here is similar to that noted by Elison and Webb [10] who observed that for small enough Weber number, single and unconfined fully developed liquid jets would broaden under the action of surface tension, even attaching themselves to the outside surface of the nozzle tube. The nozzles with the inlet modifications tended to mitigate against the development of this type of flow structure thus improving the heat transfer. However, for larger flow rates the presence of inlet only modifications has a detrimental effect on heat transfer as noted. Conversely, the presence of a chamfered outlet leads to enhancements in heat transfer of between 4 and 8% over the vast majority of the flow rate range. Between flow rates of 9 and 11 L/min, the contoured inlet/outlet and chamfered inlet/outlet

nozzles both begin to experience heat transfer coefficients that are 5-10% greater than that of the straight nozzle, and continue to do so for the remainder of the investigated flow rate range. It is not immediately obvious as to why the presence of outlet conditions leads to an enhancement in heat transfer, however these observations could possibly be explained if one considers the nozzle development length (t/d_n) as discussed by Garimella and Nenaydykh [11]. In this study, it was argued that enhancements in heat transfer were due to the presence of a separation bubble in the nozzle. It was reasoned that, for short development lengths ($t/d_n \leq 1$), the presence of a separation bubble effectively decreases the area of the jet nozzle, therefore increasing the issuing jet velocity and consequently heat transfer. In the present study, the presence of the chamfered outlet modification effectively halves the thickness of the nozzle plate to $t/d_n \approx 1.5$. Unfortunately, the present experimental set-up did not facilitate the evaluation of the inlet separation bubble length. However, as Garimella and Nenaydykh [11] only discussed the separation bubble in the case of singular jets, it is not inconceivable to expect a greater bubble length due to interactions in the plenum as the flow divides into multiple jets before passing through the nozzle array. If the separation bubble length was in the region of $t/d_n \approx 1.5$, the chamfered outlet nozzle would experience a constriction in its effective area, leading to increases in jet velocity, and consequently heat transfer.

As noted by Webb and Ma [5], in the case of free-surface liquid jet impingement, there is a scarce amount of work in the literature dealing with the effects of a liquid layer on heat transfer to the impinging jets. From results obtained in the present study, it seems that once a liquid layer begins to develop, nozzles with outlet modifications experience enhancements in heat transfer. In the absence of flow visualization techniques it is unclear as to why these configurations experience enhanced heat transfer, however it is speculated that the nozzle shapes lead to further

contraction of the jet upon exiting the nozzle. This will lead to increased velocity which may be better able to penetrate the liquid layer, striking the heater surface at a greater velocity and therefore leading to heat transfer enhancement.

Fig. 6 illustrates the corresponding relationships between pressure drop and volumetric flow rate, and again contains an embedded graph illustrating the ratios between the pressure drops of the modified arrays to those of the straight nozzle. Reductions in pressure drop are experienced by both arrays with inlet-only modifications, with the contoured inlet nozzle performing best with reductions exceeding 40% at low volumetric flow rates and in the region of 15-20% for higher flow rates. For the low flow rates the difference is explained in terms of the inlet modification nozzles mitigating the lateral merger of the jets thus establishing a more favourable flow regime with respect to heat transfer and pressure drop. For the higher flow rates the differences in pressure drop between the two modified inlet only conditions can be explained if one considers the work by Brignoni and Garimella [17]. It was reported that inlet chamfers with the largest chamfer angle (to the normal) and deepest chamfer depth yielded the lowest pressure drops. This was attributed to the removal of the sharp corner at the inlet, leading to the alleviation of the vena contracta within the nozzle. In the current study, the large depth and curved nature of the contoured inlet nozzle ensured no sharp corners were present, explaining the excellent decreases in pressure drop.

Due to a transverse pressure gradient between the edge and centre of the nozzle, a region termed the vena contracta develops a small distance after the orifice exit. The increased pressure at the centre of the jet causes it to contract leading to increased velocity. This is typically characterized by the contraction coefficient (C_c). Similarly, the velocity coefficient (C_v) is the ratio of the velocity at the vena contract to the velocity at the nozzle exit. The discharge coefficient (C_d) describes the effect that the

nozzle geometry has on the area and velocity of a jet exiting the nozzle. It is related the product of the contraction coefficient and velocity coefficient. Royne and Dey [25] related the pressure drop through a nozzle to the discharge coefficient through,

$$\Delta P = \frac{1}{2}\rho V_2^2 = \frac{1}{2}\rho \frac{\dot{V}^2}{C_d A_2^2} = \rho \dot{V}^2 \frac{8}{N^2 \pi^2 C_d^2 d_n^4} \tag{12}$$

It was further reported that the contraction coefficient varies from $C_c \approx 0.6$, for a perfectly sharp lip, to $C_c \approx 1$ for bell-mouthed opening. The variation in the contraction coefficients is due to the presence of a separation bubble within the nozzle, with smaller bubbles leading to greater contraction coefficients. The pressure drop results for the nozzles with chamfered outlet, chamfered inlet/outlet and contoured inlet/outlet modifications indicate pressure drop increases of up to 15%, suggesting small discharge coefficients. These findings further strengthen the belief that a separation bubble is present within the nozzles.

4.3 Modified Nozzle Geometries: Confined-Submerged Results

Fig. 7 depicts the relationship between the average heat transfer coefficient and volumetric flow rate for the confined-submerged jet arrangement. Again, the heat transfer coefficient ratios of the modified nozzles and straight nozzle are included in the figure. The chamfered inlet/outlet nozzle array is seen to experience a sustained enhancement in heat transfer of up to 10% beyond a flow rate of $\dot{V} \approx 9$ L/min. It is thought that this is due to the sharp corners within the nozzles which cause turbulence of enhanced magnitude within the jets, with increasing intensity at higher flow rates. This is in line with the work of Lee and Lee [8] who found a greater dependency of Nu_o on Re for their sharp edged nozzle. Another possible explanation for the enhanced heat transfer would be the effect the outlet chamfer has on the recirculation zone between the nozzle plate, heater surface and impinging jet. However, the poor performance of

the contoured inlet/outlet and chamfered outlet nozzles seem to suggest that the latter is the most probable explanation.

Unlike in the free-surface configuration, in comparison to the straight nozzle the chamfered outlet and contoured inlet/outlet both perform unfavourably under confined-submerged conditions with decreases in heat transfer coefficient between 5 and 9%. As the effective jet diameter of these jets is thought to be decreased due to the presence of a separation bubble, an increase in the relative distance to the heater surface (H/d_n) will occur. It is therefore possible that the potential core will be dissolved before the jets strike the heater surface. Consequently the jets will be of diminished velocity leading to reductions in heat transfer to the jets. In the upper flow rate ranges, the jets issuing from the contoured inlet nozzle array experience heat transfer coefficient enhancements in the region of 3-4%. This is thought to be due to the increased stability of the jets and large discharge coefficient.

Fig. 8 illustrates the variations in pressure drop with volumetric flow rate for each array together with the ratios between the modified arrays and the straight nozzle array. In comparison to the free-surface pressure drop data, similar results are obtained with the chamfer outlet and chamfered inlet/outlet nozzles both experiencing increased pressure drops, although of decreased magnitude, in the region of 8%. The contoured inlet and chamfered inlet arrays again both experience impressive reductions in pressure drop of up to 25%. Also, unlike the free-surface data set, a marked reduction in pressure drop is observed by the contoured inlet/outlet nozzle with reductions in the region of 10%.

4.4 Pumping Power Requirements

As previously discussed the pumping power requirement of a cooling package plays an important role in its suitability for use in the cooling of electronic components.

The pumping power required to form the jets is related to the pressure drop across the nozzle plate, ΔP, and the volumetric flow rate, $\dot{V}$, by

$$Q_{pumping} = \dot{V} \Delta P \tag{13}$$

Using the flow rates, pressure drops and heat transfer coefficients recorded in sections 4.1 – 4.3, the pumping power requirement for a given heat transfer coefficient is plotted for all nozzles, both free and confined-submerged, in Fig. 9. It is immediately obvious that the submerged nozzles collectively outperform the free-surface jets. This has been previously demonstrated in the literature [23], and can be attributed to the increased heat transfer to confined-submerged jets as explained in section 4.1.

In the case of the free-surface jets it is evident that, in comparison to the straight nozzle, the significant reductions in pressure drop for the contoured inlet, and to a lesser extent the chamfered inlet nozzles, have small effects on the jet performance when the heat transfer coefficient is considered in relation to the required pumping power. The nozzles that achieve an increase in heat transfer coefficient i.e. nozzles with outlet modifications, generally do so with a penalty of increased pressure drop. Even still these nozzles experience better overall performance from a pumping power-heat transfer coefficient point of view. This can be explained by the fact that these nozzles can achieve a certain heat transfer at lower volumetric flow rates, even though the pressure drop required to form the jets is of greater magnitude. Thus it can be concluded that, for free-surface jets, nozzles that achieve increases in heat transfer coefficient are more effective than those nozzles that cause pressure drop reductions when the heat transfer coefficient for a specific pumping power cost is considered.

In the case of the confined-submerged jets only the contoured inlet and chamfered inlet/outlet nozzles experience notable enhancements in performance over the straight nozzle. Again the increases in heat transfer coefficient achieved by the chamfered inlet/outlet nozzle compensates for the minor increase in the pressure drop.

Conversely, the contoured inlet nozzle shows small relative variation in its heat transfer coefficient in combination with an impressive reduction in the pressure drop resulting in excellent overall performance. Although performing exceptionally well for free-surface jets, the contoured inlet/outlet array is possibly the worst configuration under confined-submerged conditions.

5. Conclusions

The heat transfer and pressure drop characteristics of both submerged and free-surface liquid jet arrays with modified inlet and/or outlet geometries have been investigated for a range of volumetric flow rates for a fixed number of 1.0 mm jets. With regards to heat transfer, the submerged jets exceeded the performance of their free jet counterparts. Generally, the presence of an inlet modification alone was observed to lead to decreases in pressure drop, whilst the addition of an outlet modification had an adverse effect. For free-surface jets, the addition of outlet modifications had a positive effect on heat transfer. It was found that for both free-surface and confined-submerged conditions, those nozzle configurations that caused enhancements in the heat transfer coefficient generally had a more significant improvement on the overall performance than those that caused pressure drop reductions. An exception to this was the contoured inlet nozzle configuration which, under confined-submerged conditions, was one of the highest performing jets primarily due to its ability to significantly reduce the pressure drop. From an electronics packaging standpoint, where power consumption may need to be minimized whilst achieving a given design heat transfer coefficient, the confined-submerged nozzles with contoured inlet or inlet/outlet are the suggested nozzle configurations.

Acknowledgements

This work was supported by the CTVR, a CSET of Science Foundation Ireland.

Particular gratitude is extended to Bell Laboratories Ireland.

Nomenclature

A	area (m)
C_c	contraction coefficient
C_d	discharge coefficient
C_v	velocity coefficient
d_n	jet diameter (m)
D	heater surface diameter (m)
f	friction factor (-)
H	distance between orifice plate and impingement surface (m)
$\bar{h}$	surface averaged heat transfer coefficient (W/m^2 K)
k	thermal conductivity (W/m K)
L_c	characteristic Length (m)
t	thickness of nozzle plate (m)
N	number of jets on orifice plate (-)
Nu	Nusselt number (-)
ΔP	pressure drop across nozzle plate (Pa)
Pr	Prandtl number (-)
q''	heat flux (W/m^2)
$Q_{pumping}$	pumping power (W)
Re	Reynolds number (-)
S	jet-to-jet spacing (m)
t	thickness of nozzle plate (m)
T	temperature (ºC or K)
V_n	nozzle exit velocity (m/s)
$\dot{V}$	volumetric flow rate (m^3/s)
z	location of thermocouple (m)

Subscripts

c	vena contracta
d	discharge
f	fluid

film	film temperature
jet	jet
n	nozzle
s	surface
t	top thermocouple in block
v	velocity
2	nozzle exit

Greek

μ	dynamic viscosity (Ns/m^2)
ρ	density (kg/m^3)
υ	kinematic viscosity (m^2/s)

References

[1] DTI Global Watch Mission Report, Developments and trends in thermal management technologies - a mission to the USA, December 2006.

[2] W. Schutt, Continuous-flow jet-heating furnaces for heating and heat-treatment of aluminium forgings and castings, Gaswaerme International 56 (2007) 290-292.

[3] R.S. Bunker, Gas turbine heat transfer: Ten remaining hot gas path challenges, Journal of Turbomachinery 129 (2007) 193-201.

[4] M. Fabbri and V.K. Dhir, Optimized heat transfer for high power electronic cooling using arrays of microjets, Journal of Heat Transfer 127 (2005) 760-769.

[5] B.W. Webb and C.F. Ma, Single-phase liquid jet impingement heat transfer, Advances in Heat Transfer 26 (1995) 105-217.

[6] J. A. Fitzgerald and S.V. Garimella, A study of the flow field of a confined and submerged impinging jet, International Journal of Heat and Mass Transfer 41 (1998) 1025-34.

[7] T.L. Lupton, D.B. Murray, and A.J. Robinson, The effect of varying confinement levels on the heat transfer to a miniature impinging air jet, Eurotherm 2008, Eindhoven, Netherlands.

[8] J. Lee and S.J. Lee, The effect of nozzle configuration on stagnation region heat transfer enhancement of axisymmetric jet impingement, International Journal of Heat and Mass Transfer 43, (2000) 3497-3509.

[9] J. Stevens and B.W. Webb, Local heat transfer coefficients under an axisymmetric, single-phase liquid jet, Journal of Heat Transfer 113 (1991) 71-78.

[10] B. Elison and B.W. Webb, Local heat transfer to impinging liquid jets in the initially laminar, transitional, and turbulent regimes, International Journal of Heat and Mass Transfer 37 (1994) 1207-1216.

[11] S.V. Garimella and B. Nenaydykh, Nozzle-geometry effects in liquid jet impingement heat transfer, International Journal of Heat and Mass Transfer, 39 (1996) 2915-2923.

[12] S.V. Garimella and R. A. Rice, Confined and submerged liquid jet impingement heat transfer, Journal of Heat Transfer 117 (1995) 871-877.

[13] J. Stevens and B.W. Webb, Measurements of the free surface flow structure under an impinging, free liquid jet, Journal of Heat Transfer 114 (1992) 79-84.

[14] D.H. Lee, J. Song, and M.C. Jo, The Effects of Nozzle Diameter on Impinging Jet Heat Transfer and Fluid Flow, Journal of Heat Transfer 126 (2004) 554-557.

[15] Z.Q. Lou, A.S. Mujumdar, and C. Yap, Effects of geometric parameters on confined impinging jet heat transfer, Applied Thermal Engineering 25 (2005) 2687-2697.

[16] T.S. O'Donovan and D.B. Murray, Jet impingement heat transfer - Part I: Mean and root-mean-square heat transfer and velocity distributions, International Journal of Heat and Mass Transfer 50 (2007) 3291-3301.

[17] L.A. Brignoni and S.V. Garimella, Effects of nozzle-inlet chamfering on pressure drop and heat transfer in confined air jet impingement, International Journal of Heat and Mass Transfer 43, (2000) 1133-1139.

[18] H. Martin, Heat and Mass Transfer Between Impinging Gas Jets and Solid Surfaces, Advances in Heat Transfer 13 (1977) 1-60.

[19] K. Jambunathan, E. Lai, M.A. Moss, and B. L. Button, A review of heat transfer data for single circular jet impingement, International Journal of Heat and Fluid Flow 13 (1992) 106-115.

[20] R. J. Goldstein and J. F. Timmers, Visualization of heat transfer from arrays of impinging jets, International Journal of Heat and Mass Transfer 25 (1982) 1857-1868.

[21] D.J. Womac, F.P. Incropera, and S. Ramadhyani, Correlating equations for impingement cooling of small heat sources with multiple circular liquid jets, Journal of Heat Transfer 116 (1994) 482-486.

[22] Y. Pan and B.W. Webb, Heat transfer characteristics of arrays of free-surface liquid jets, Journal of Heat Transfer 117 (1993) 878-883.

[23] A. J. Robinson and E. Schnitzler, An experimental investigation of free and submerged miniature liquid jet array impingement heat transfer, Experimental Thermal and Fluid Science 32 (2007) 1-13.

[24] N.T. Obot and T.A. Trabold, Impingement heat transfer within arrays of circular jets: part 1 - effects of minimum, intermediate, and complete crossflow for small and large spacings, Journal of Heat Transfer 109 (1987) 872-879.

[25] A. Royne and C.J. Dey, Effect of nozzle geometry on pressure drop and heat transfer in submerged jet arrays, International Journal of Heat and Mass Transfer 49 (2006) 800-804.

[26] S. Petrovic, A.J. Robinson, and R.L. Judd, Marangoni heat transfer in subcooled nucleate pool boiling, International Journal of Heat and Mass Transfer 47 (2004) 5115-5128.

[27] K. Garrett and B.W. Webb, The effect of drainage configuration on heat transfer under an impinging liquid jet array, Journal of Heat Transfer 12 (1999) 803-810.

[28] I.D. Faux, M. J. Pratt, Computational Geometry for Design and Manufacture (Mathematics and Its Applications), Halsted Press New York, NY, USA, 1979.

Figure Captions

Figure 1: Schematic of jet impingement heat transfer apparatus.

Figure 2: Schematic of test chamber.

Figure 3: Reynolds number vs. Nusselt number for straight nozzles.

Figure 4: Reynolds number vs. friction factor for straight nozzles.

Figure 5: Average heat transfer coefficient vs. volumetric flow rate for free-surface jet arrays.

Figure 6: Pressure drop vs. volumetric flow rate for free-surface jet arrays.

Figure 7: Average heat transfer coefficient vs. volumetric flow rate for confined-submerged jet arrays.

Figure 8: Pressure drop ratio vs. volumetric flow rate for confined-submerged jet arrays.

Figure 9: Pumping power vs. average heat transfer coefficient for all nozzles under free and confined-submerged conditions.

Table Captions

Table 1: Nozzle characteristics.

Table 2: Experimental uncertainties.

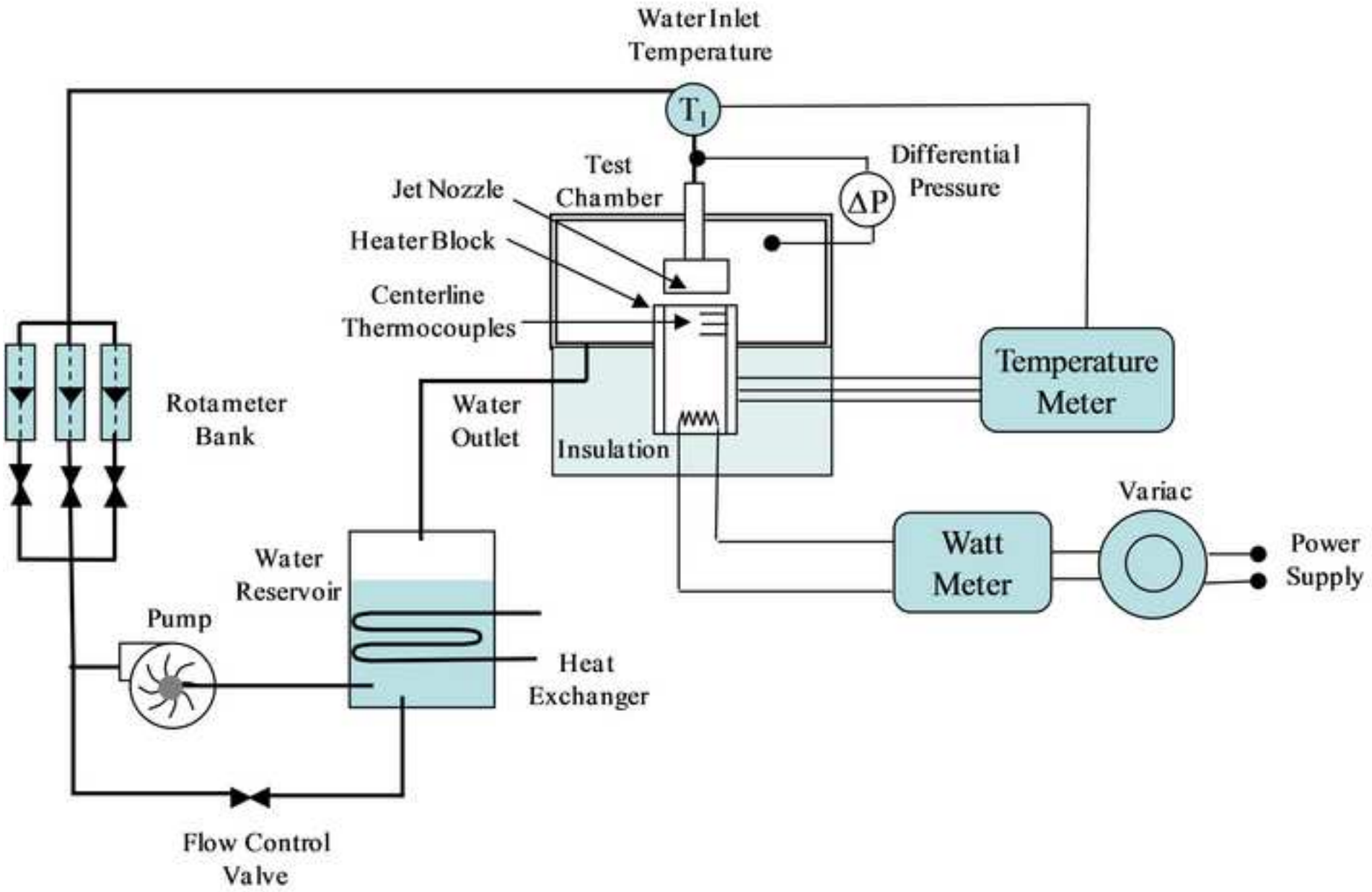
Water Inlet Temperature
T_1
Test Chamber
Jet Nozzle
Heater Block
Centerline Thermocouples
Differential Pressure
ΔP
Temperature Meter
Rotameter Bank
Water Outlet
Insulation
Variac
Watt Meter
Power Supply
Water Reservoir
Pump
Heat Exchanger
Flow Control Valve

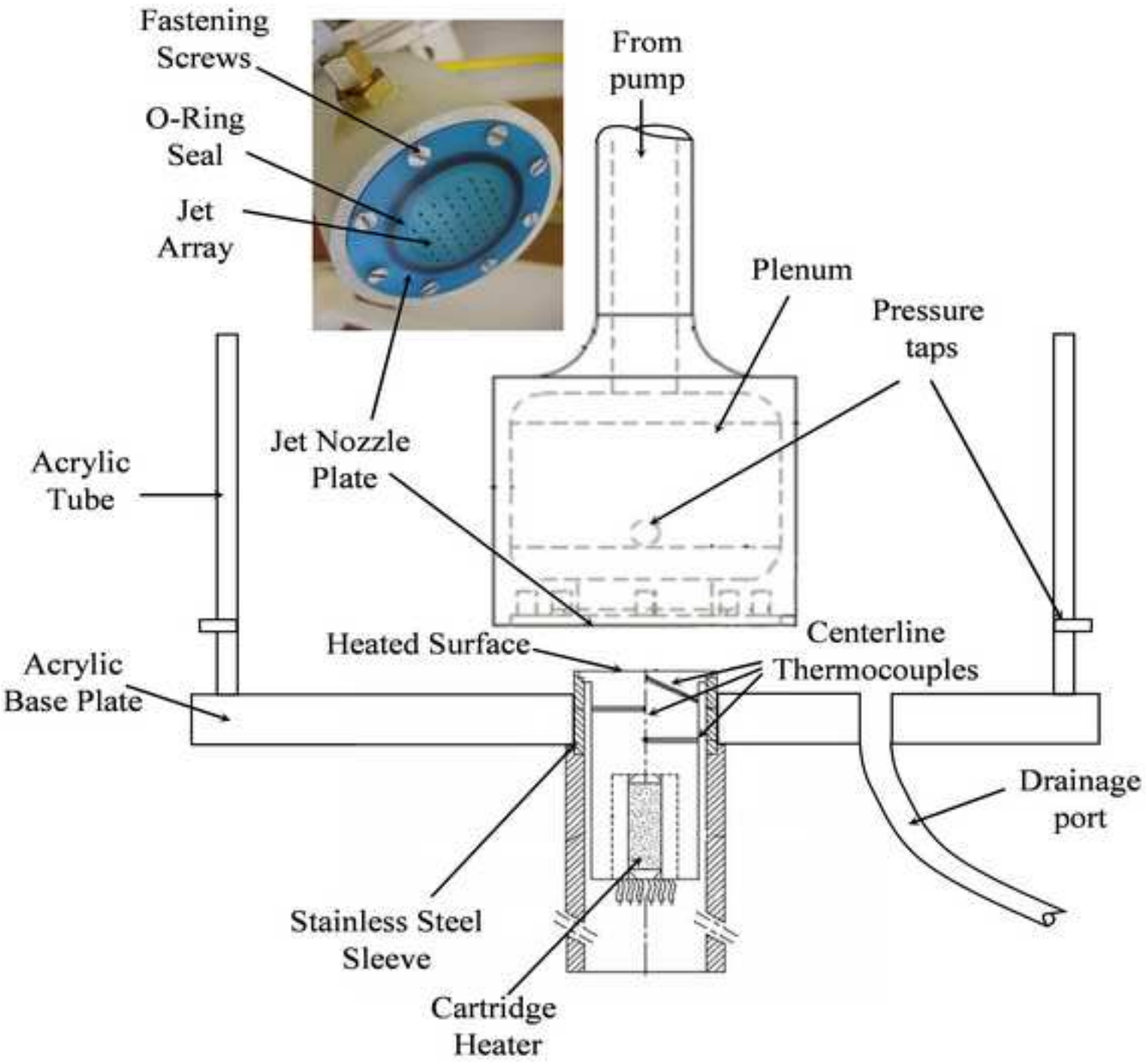
Fastening Screws
O-Ring Seal
Jet Array
From pump
Plenum
Pressure taps
Jet Nozzle Plate
Acrylic Tube
Heated Surface
Centerline Thermocouples
Acrylic Base Plate
Drainage port
Stainless Steel Sleeve
Cartridge Heater

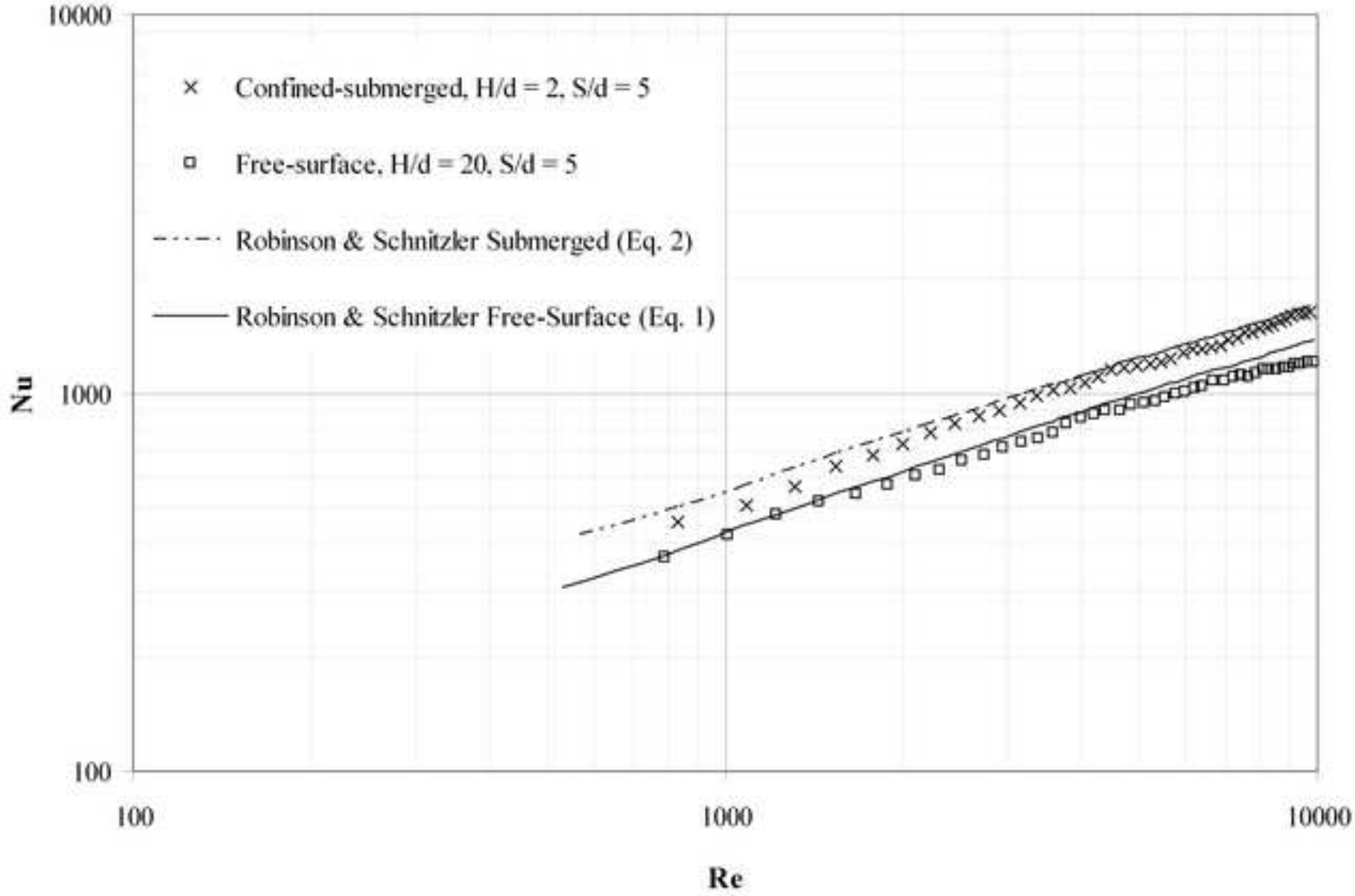
10000
1000
100
Nu
100
1000
10000
Re
Confined-submerged, H/d = 2, S/d = 5
Free-surface, H/d = 20, S/d = 5
Robinson & Schnitzler Submerged (Eq. 2)
Robinson & Schnitzler Free-Surface (Eq. 1)

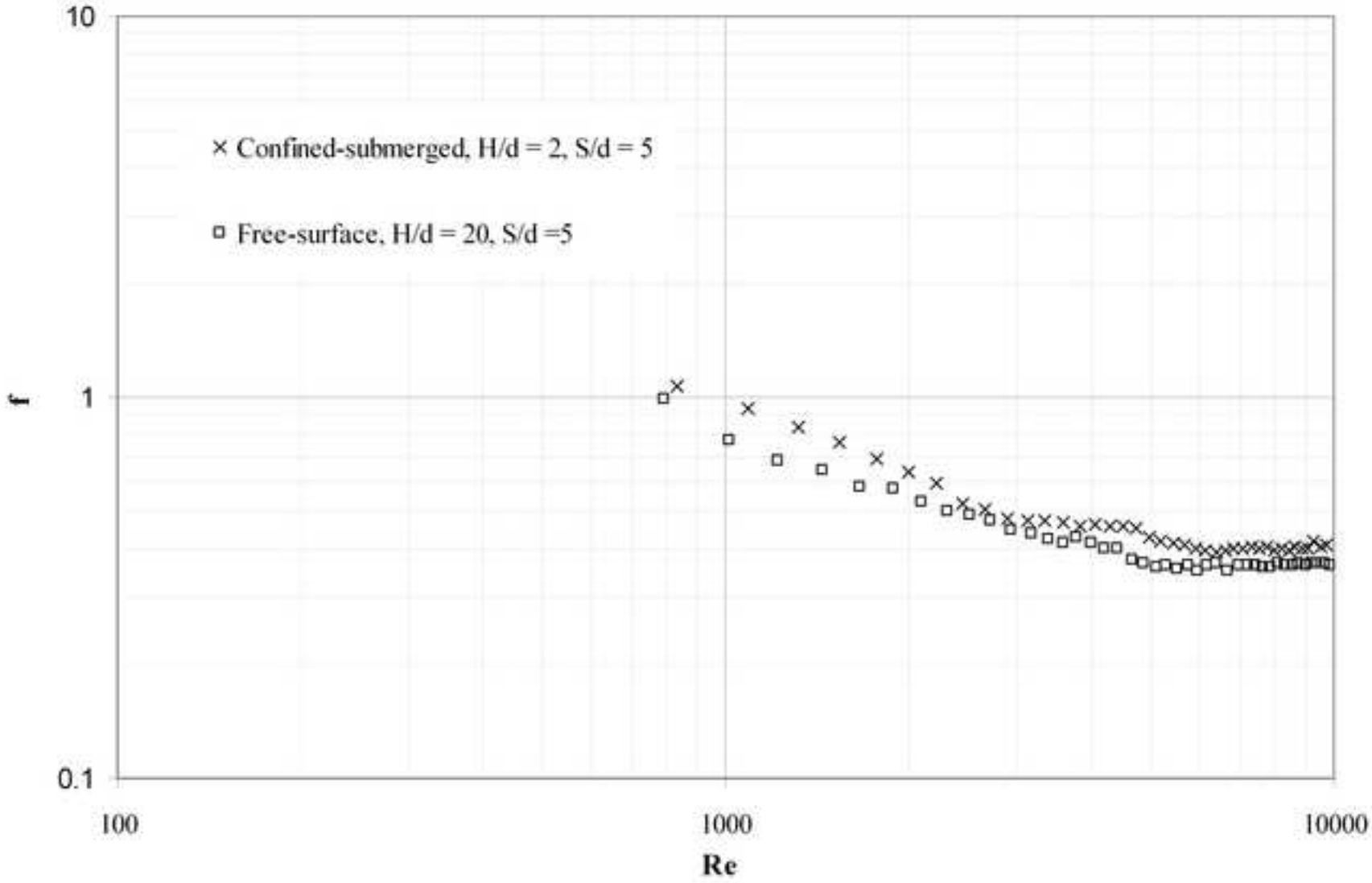
10
1
0.1
f
× Confined-submerged, H/d = 2, S/d = 5
□ Free-surface, H/d = 20, S/d =5
100
1000
10000
Re

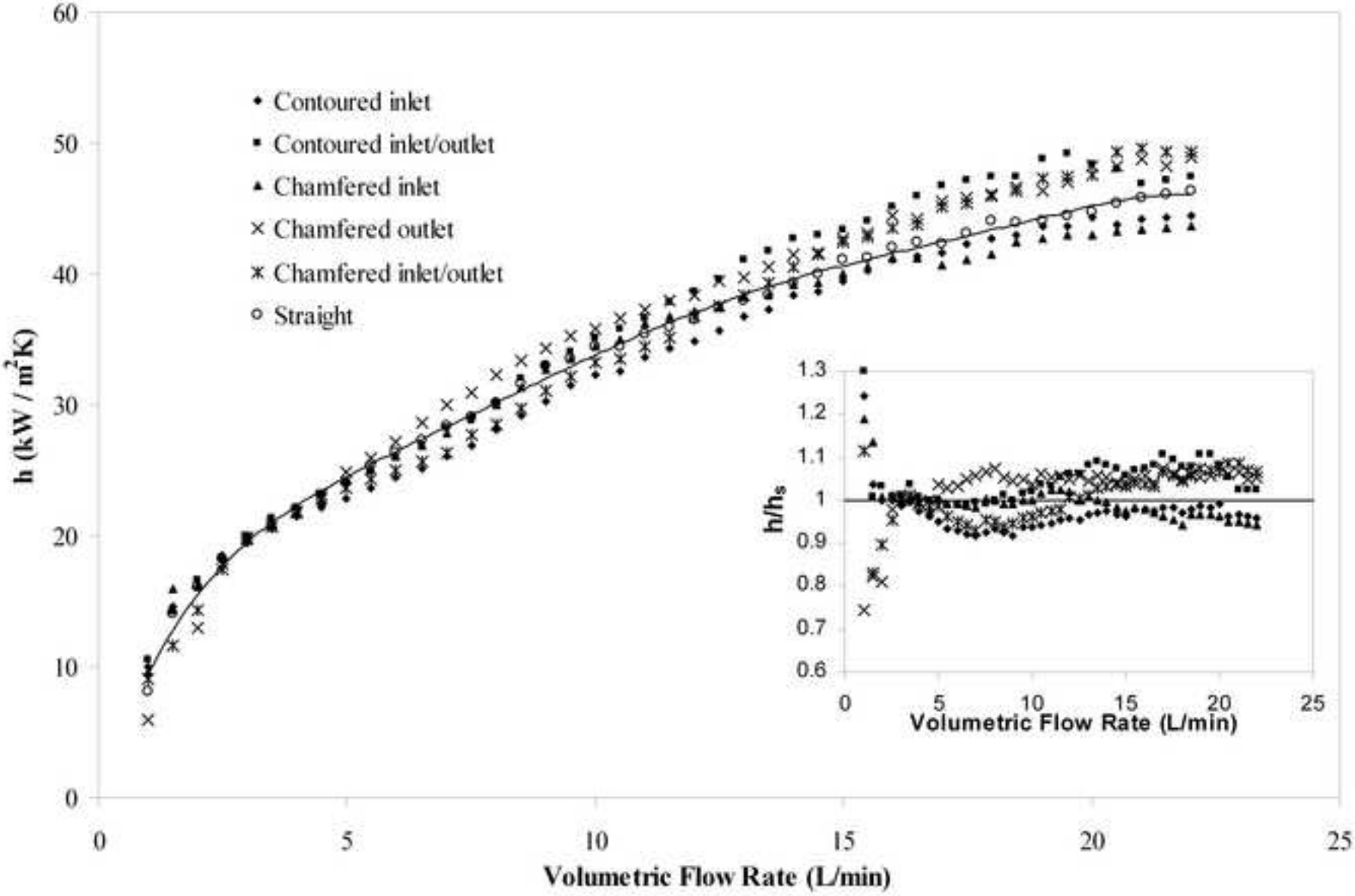
Contoured inlet
Contoured inlet/outlet
Chamfered inlet
Chamfered outlet
Chamfered inlet/outlet
Straight
h (kW / m²K)
Volumetric Flow Rate (L/min)
h/hs
Volumetric Flow Rate (L/min)

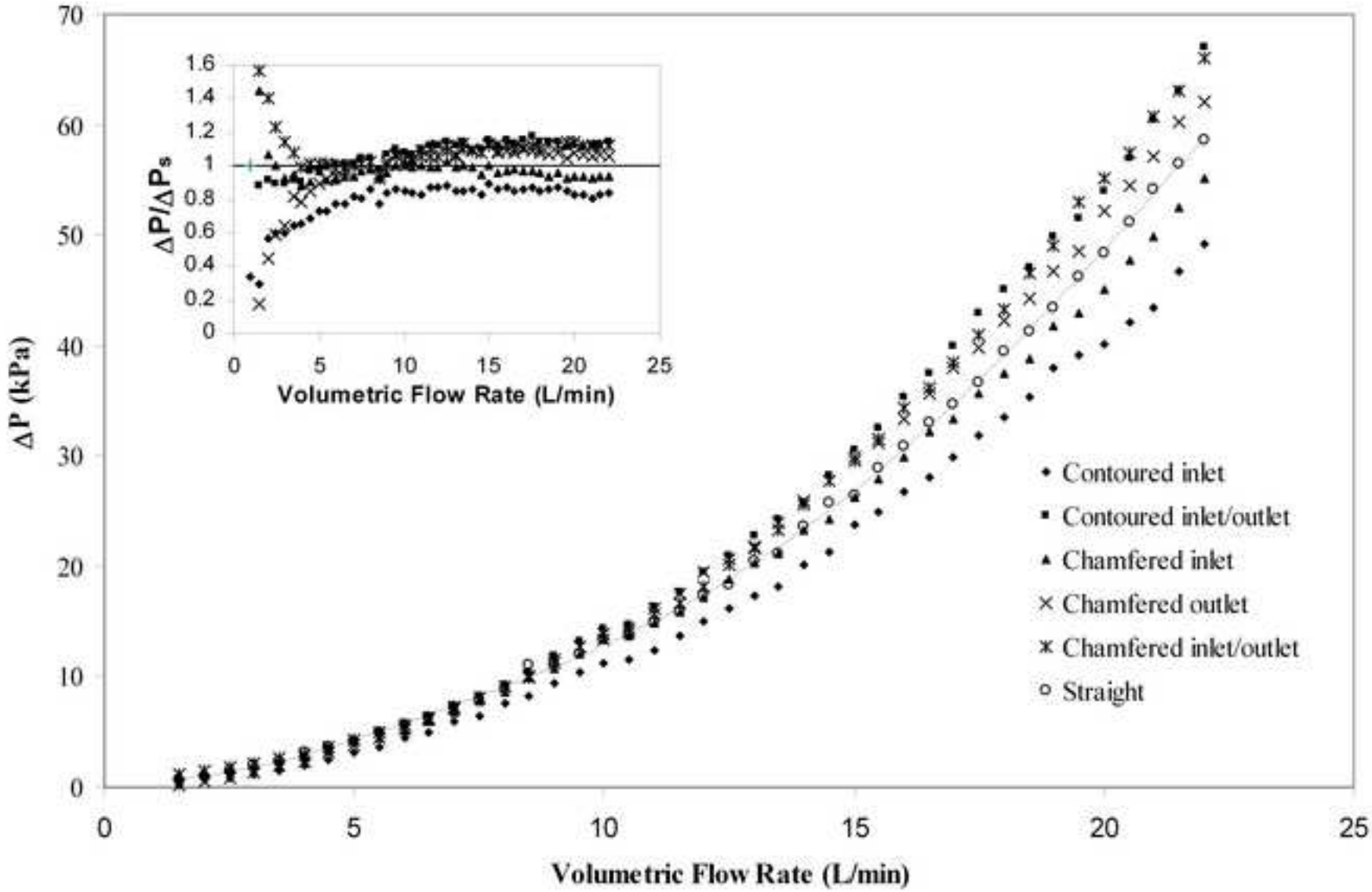
ΔP (kPa)
Volumetric Flow Rate (L/min)
0
10
20
30
40
50
60
70
0
5
10
15
20
25
Contoured inlet
Contoured inlet/outlet
Chamfered inlet
Chamfered outlet
Chamfered inlet/outlet
Straight
ΔP/ΔPs
0
0.2
0.4
0.6
0.8
1
1.2
1.4
1.6
Volumetric Flow Rate (L/min)

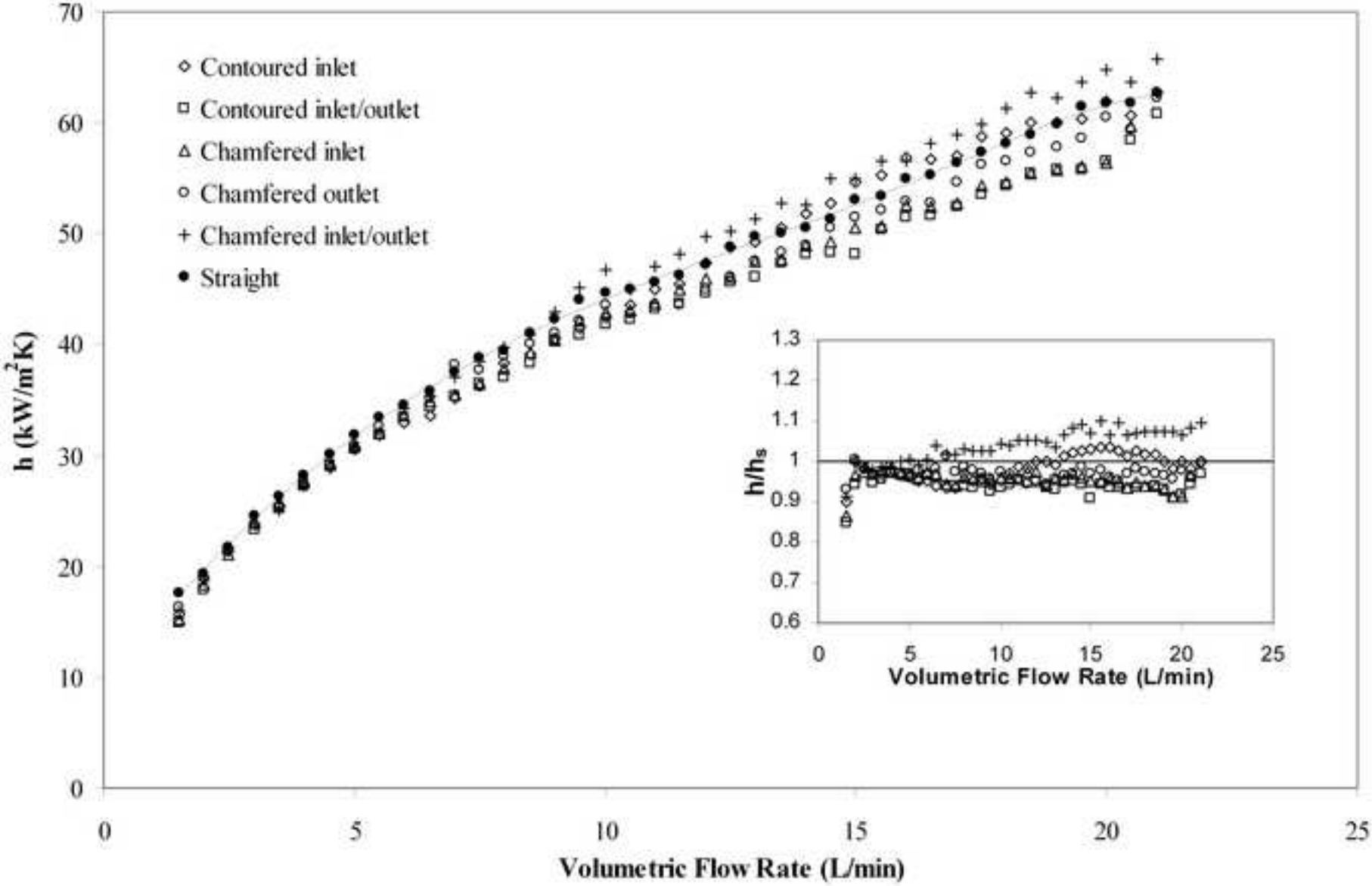
Contoured inlet
Contoured inlet/outlet
Chamfered inlet
Chamfered outlet
Chamfered inlet/outlet
Straight
h (kW/m²K)
Volumetric Flow Rate (L/min)
h/hs
Volumetric Flow Rate (L/min)

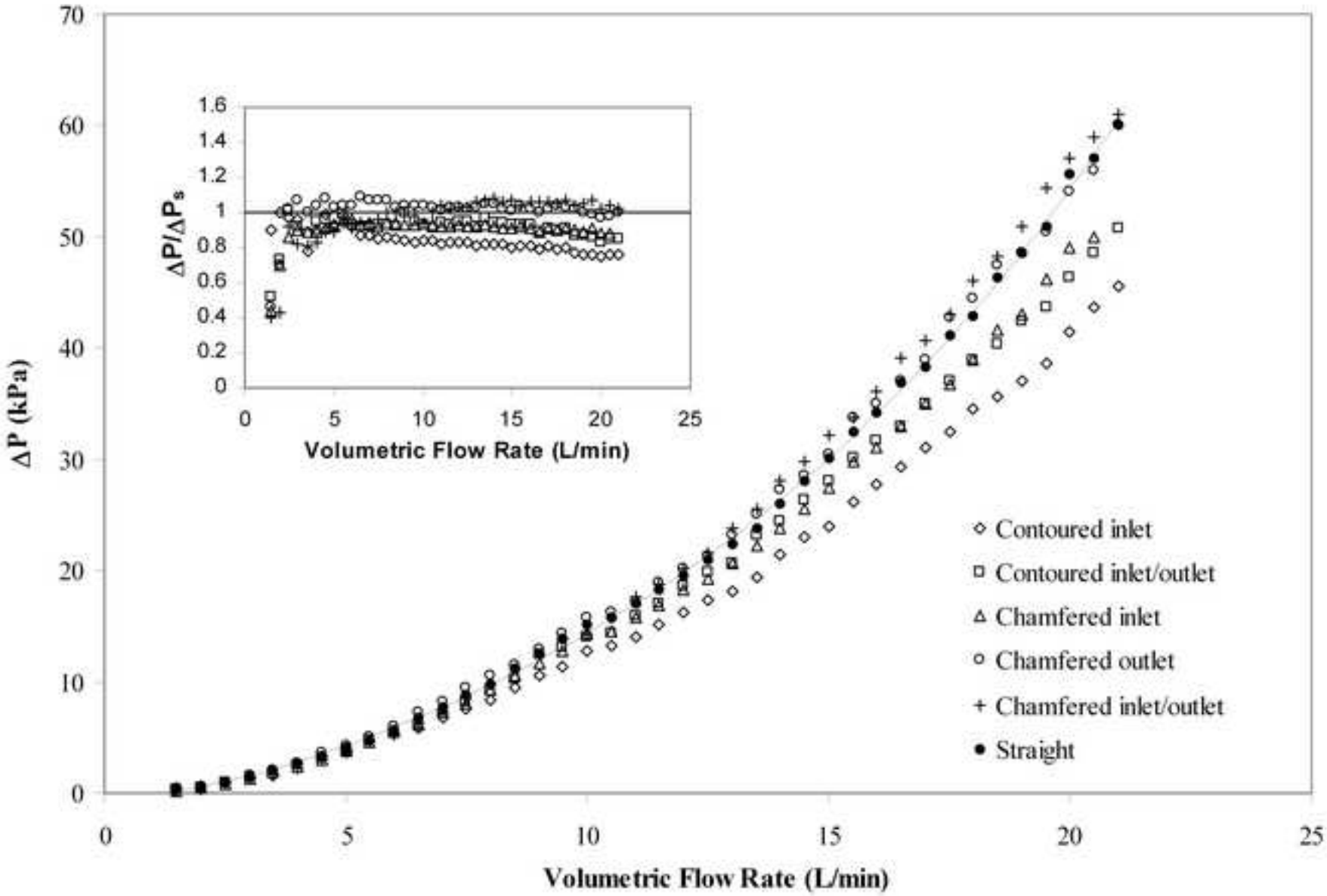
ΔP (kPa)
Volumetric Flow Rate (L/min)
ΔP/ΔPs
Volumetric Flow Rate (L/min)
Contoured inlet
Contoured inlet/outlet
Chamfered inlet
Chamfered outlet
Chamfered inlet/outlet
Straight

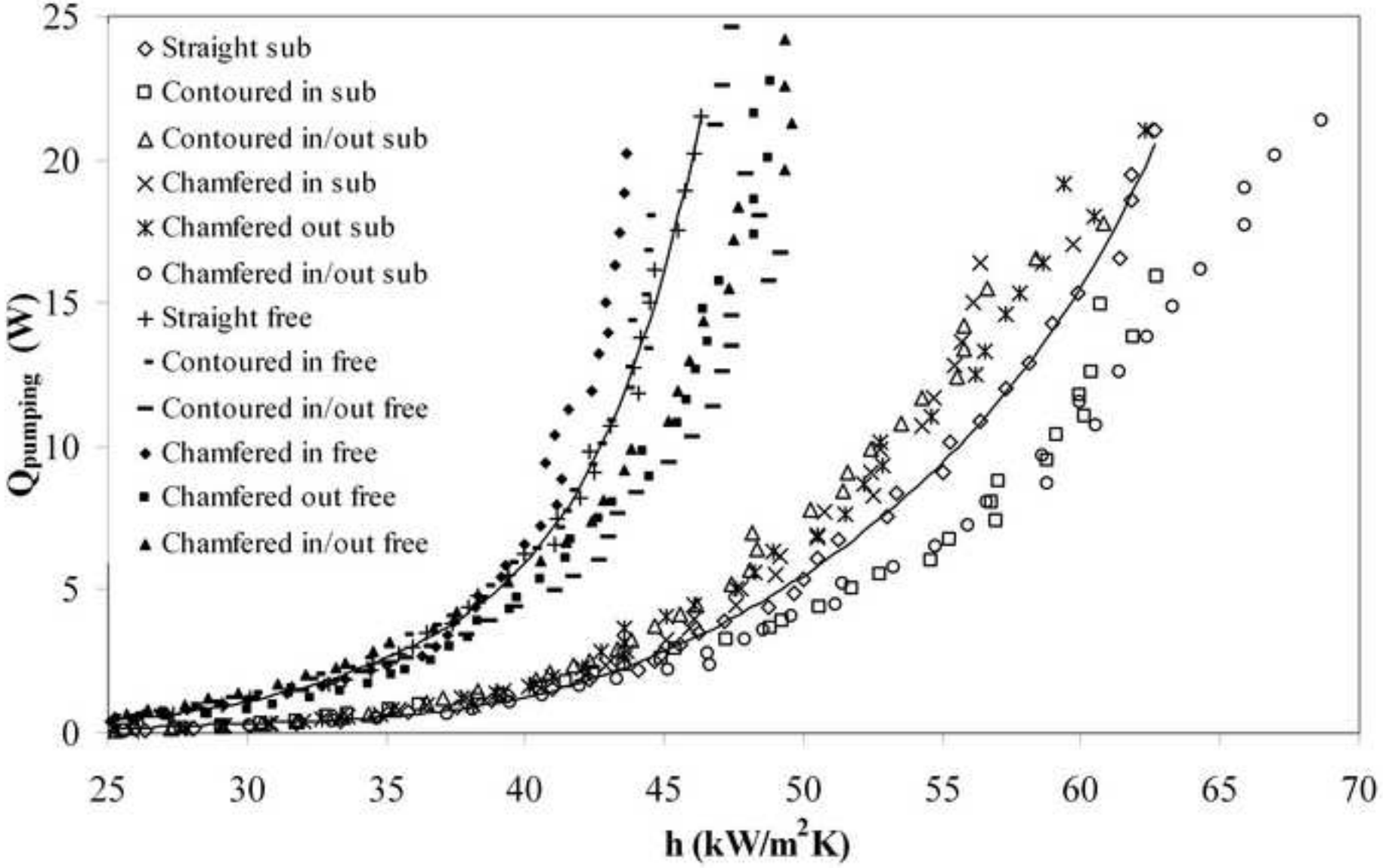
Straight sub
Contoured in sub
Contoured in/out sub
Chamfered in sub
Chamfered out sub
Chamfered in/out sub
Straight free
Contoured in free
Contoured in/out free
Chamfered in free
Chamfered out free
Chamfered in/out free
Q pumping (W)
h (kW/m2K)
0
5
10
15
20
25
25
30
35
40
45
50
55
60
65
70

Name	**Configuration**
Straight	
Contoured Inlet	
Contoured Inlet/Outlet	
Chamfered Inlet	
Chamfered Outlet	
Chamfered Inlet/Outlet	

Nu_L	Re_{dn}		f	
	(2LPM)	*(9LPM)*	(2LPM)	(9LPM)
7%	10%	5%	20%	12%